GEOLOGICA CARPATHICA, OCTOBER 2005, 56, 5, 455–460

Shaping of clay fragments during transport: a theoretical model

JIŘÍ FAIMON

Institute of Geological Sciences, Faculty of Sciences, Masaryk University, Kolářská 2, 611 37 Brno, Czech Republic;
faimon@sci.muni.cz

(Manuscript received July 22, 2004; accepted in revised form March 17, 2005)

Abstract: Irregular blocks of cohesive clay (**IBC**) are transformed into *spherical clay balls* (**SCB**) during transport across a sedimentary basin bed by runoff. This transformation is controlled by rotation of the **IBC** about a randomly changing axis. During this process, deformation dominates; abrasion is less significant. Based on a theoretical model, the equation describing **SCB** formation, $\Psi = 1 - (1 - \Psi_0)e^{-\frac{k\lambda}{\pi d_{ef}}}$, was derived in terms of the **SCB** instantaneous sphericity, Ψ, the **IBC** initial sphericity, Ψ_0, the transport length, λ, and the effective diameter, $\mathbf{d}_{ef}$. The equation was validated with the new data set obtained from **IBC/SCB** distribution along the transport path on the bed of an artificial basin (sandpit quarry). The coefficient **k** was found to be 2.9×10^{-4} and 4.8×10^{-4} for the shaping of two kinds of clays, respectively. Based on the proposed model, the length of transport can be estimated if sphericity and effective diameter are known. Despite the verification in the artificial setting, the presented model is valid also for the natural environment of various clay rich cliffs or scarps.

Key words: Czech Republic, Rudice Formation, modelling, recent process, sedimentology, basin bed, clay ball.

Introduction

The formation of rounded clay pebbles (known as *clay balls* or *mud balls*) was described in various environments by many authors (e.g. Haas 1927; Bell 1940; Karcz 1969; Picard & High 1973; Ojakangas & Thompson 1977; Collinson & Thompson 1982; Kale & Awasthi 1993; Tanner 1996; Faimon & Nehyba 1998a,b; Hindson & Andrade 1999; Sholokhov & Tiunov 2002).

Recently, Faimon & Nehyba (2004) presented the semi-empirical equation,

$$\Psi = 1 - (1 - \Psi_0)10^{-8.9\times10^{-5}\frac{\lambda}{d_{ef}}}, \quad (1)$$

describing the **SCB** formation (Ψ is instantaneous sphericity, Ψ_0 is initial sphericity, λ is transport length, and $\mathbf{d}_{ef}$ is effective diameter of the relevant clay ball). Now, a theoretical model has been proposed, based on which the former equation was verified by an exact derivation. The new model was validated with the data collected in a small artificial sedimentary basin (sandpit quarry, the Rudice-Seč, Czech Republic, see the map on Fig. 1).

Pit characteristics

The sandpit originated during the industrial mining of Lower Cretaceous deposits known as the Rudice Formation. These deposits, more than 100 m thick, are redeposited products of kaolinite-laterite weathering of non-carbonate rocks (Brno Massif granitoids, Lower Carboniferous siliciclastics) and carbonate rocks (Jurassic limestones with chert and quartz geodes; see Bosák et al. 1976). The deposits consist of quartz sands (fine to medium grained with minor sandy gravel) with abundant

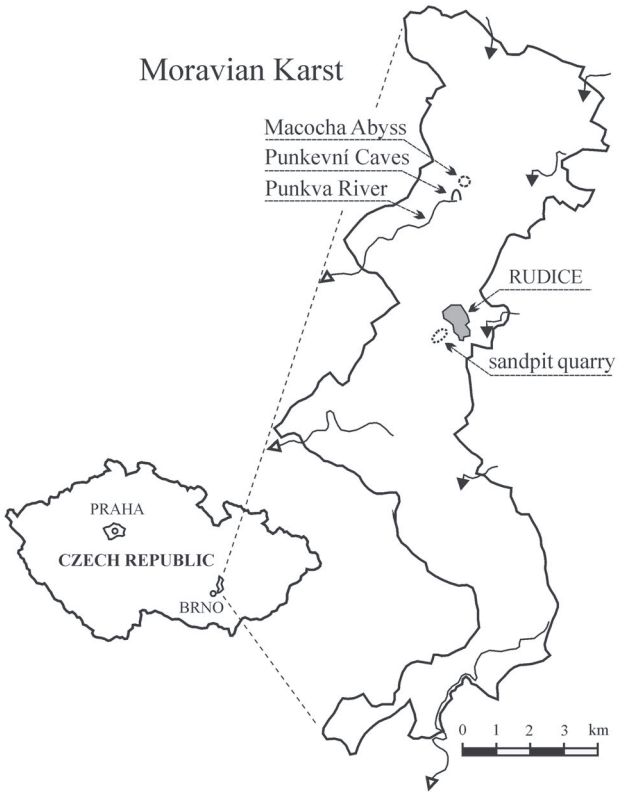

Fig. 1. Location map of the Moravian Karst and Rudice site.

chert clasts, red coloured ferruginous sandstones and multicoloured clays (dominance of kaolinite). The sandpit was described in detail by Faimon & Nehyba (2004).

Clay characteristics

Red and white clays are typical constituents of the clay balls. Their chemical and mineralogical compositions are given in Tables 1 and 2, respectively. Both clays include predominantly kaolinite and quartz, together with small amounts of other phases.

Processes on quarry slopes

The studied area is situated in the northwest–west part of the quarry. During heavy rains, small *irregular blocks of clay* (**IBC**) are released from steep slopes by gully erosion and quickly transported to the steep slope base by runoff and gravitation. The mechanism of the **IBC** formation and release was discussed in detail by Faimon & Nehyba (2004).

Runoff rolls the **IBC** deeper into the basin in an ephemeral shallow streambed (0.3–2.0 m wide and up to 0.4 m deep) that gradually transforms into a fan (up to 10 m wide and 0.2 m high). The distance from the steep slope base to a depositional base is about 135 m with relative elevation change of 5 m. Based on a rotation about a randomly changed axis, the **IBC** are rounded into *spherical clay balls* (**SCB**). These **SCB** stay spread along the transport path as the runoff has decayed.

Methods

The shape of **IBC/SCB** was expressed by the *projection sphericity,* Ψ (Sneed & Folk 1958) defined by the equation

$$\Psi = \sqrt[3]{S^2/(L\,I)}\,. \qquad (2)$$

The symbols **L**, **I**, and **S** stand for the long, intermediate, and short **IBC/SCB** dimensions in meters, respectively. The size of **IBC/SCB** was quantified by an "effective diameter", $\mathbf{d}_{ef}$ [m],

$$d_{ef} = \sqrt[3]{L\,I\,S}\,, \qquad (3)$$

where **L**, **I,** and **S** have the former meaning. The $\mathbf{d}_{ef}$ relates to the cube edge that has the same volume as the block **L**×**I**×**S** apprehending the **IBC/SCB**. The $\mathbf{d}_{ef}$ is roughly the same for the objects of the same volumes and, thus, it is independent on the **IBC/SCB** shape.

Results

The instantaneous **IBC/SCB** distribution along the transport path was obtained on one day: August 26, 2001. The frequency histogram of total 322 **IBC/SCB** is shown in Fig. 2. The white **IBC/SCB** are more abundant (243 pieces), as visible from a comparing the two areas

Table 1: Chemical composition of the clays (analyst P. Kadlec).

	red clay [wt. %]	white clay [wt. %]
H_2O	8.61	13.06
SiO_2	54.94	46.80
TiO_2	2.45	1.12
Al_2O_3	25.89	37.29
Fe_2O_3	5.68	0.38
FeO	0.11	0.06
MnO	0.01	0.01
CaO	0.68	0.74
MgO	0.08	0.01
K_2O	0.62	0.06
Na_2O	0.16	0.00
CO_2	0.67	0.44
P_2O_5	0.09	0.04

Table 2: Mineral composition of the clays. The phases were qualitatively detected by X-ray diffraction (Stady P, analyst V. Vávra) and then quantitatively calculated from the chemical composition.

	red clay [mol. %]	white clay [mol. %]
kaolinite	36.0	85.5
quartz	54.3	10.5
calcite	1.8	3.1
K-feldspar	1.9	0.3
albite	0.8	0.0
hematite	5.2	0.6

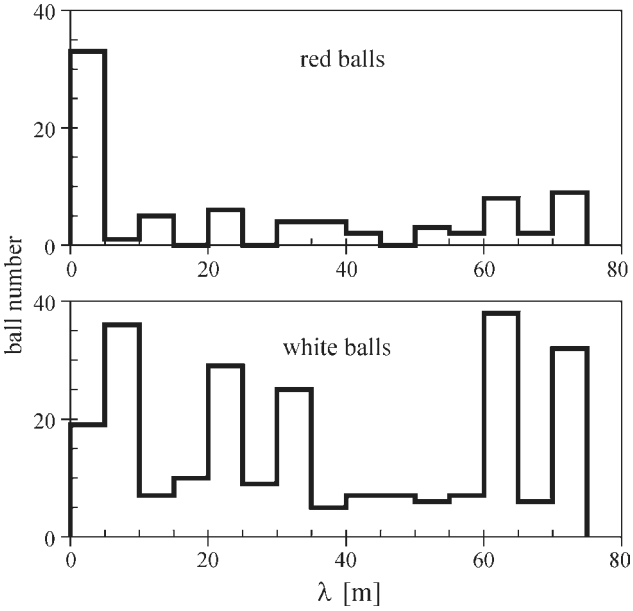

Fig. 2. Frequency histogram of clay ball distribution along transport path.

below the histogram contours. The large occurrence of **SCB** at 60–65 and 70–75 m indicates that the distribution copies, to some extent, the basin bed morphology (local inclinations and streambed spreading).

The frequency histogram of the clay ball sphericity Ψ is presented in Fig. 3. The sphericity is scattered around the value of 0.75; the mean values are 0.738 and 0.752, the medians are 0.757 and 0.763 for the red and white **IBC/SCB**, respectively. The sphericity exceeding the

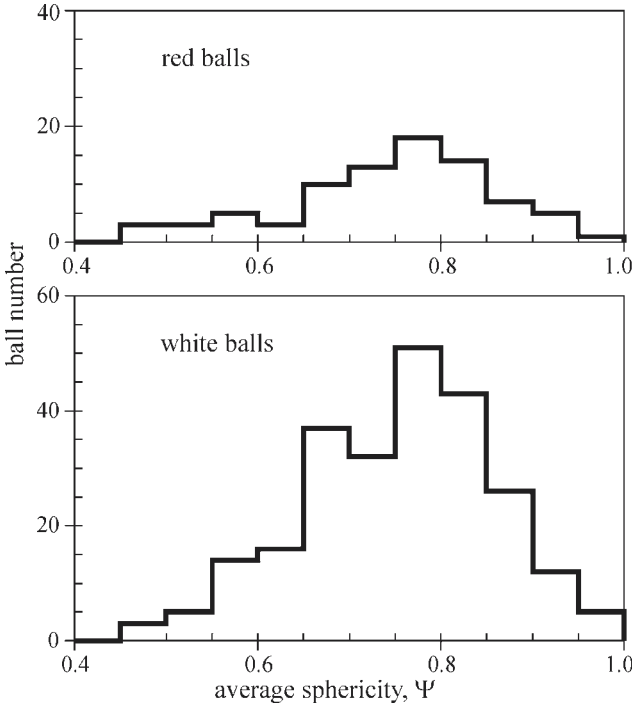

Fig. 3. Frequency histogram of clay ball sphericity.

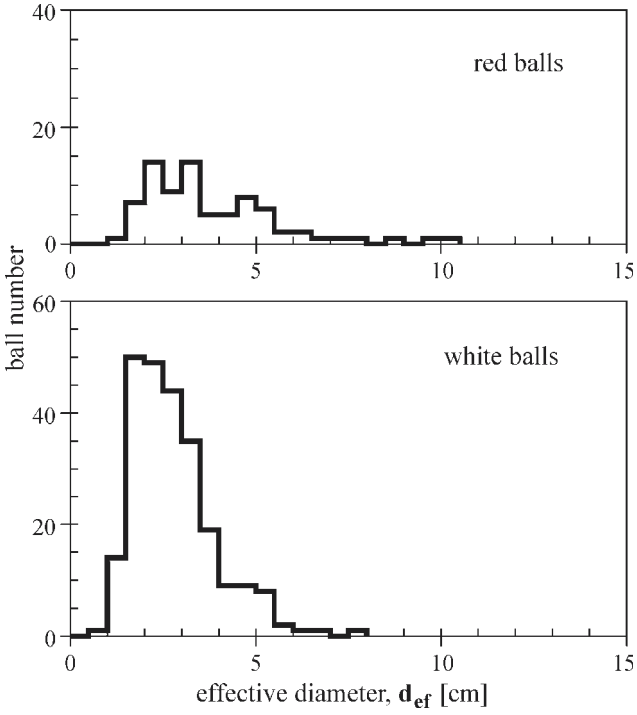

Fig. 4. Frequency histogram of clay ball effective diameter.

value of 0.90 indicates nearly ideal spherical shape of some **SCB**. The sphericity of the most irregular objects does not go under 0.45.

The frequency histogram of the effective diameters, $\mathbf{d_{ef}}$, is demonstrated in Fig. 4. The typical $\mathbf{d_{ef}}$ of **IBC/SCB** was 1 to 5.5 cm. The mean diameter and median of the red **IBC/SCB** were 3.7 and 3.2 cm, the mean diameter and medians of the white **IBC/SCB** were 2.8 and 2.6 cm, respectively. In fact, solely the **IBC/SCB** exceeding 0.5 cm in diameter were monitored.

The dependence of sphericity $\mathbf{\Psi}$ on the distance from steep slope base $\boldsymbol{\lambda}$ is shown in Fig. 5. The positive slopes 0.0011 and 0.0013 m^{-1} for the red and white **IBC/SCB**, respectively, indicate the slight increase of $\mathbf{\Psi}$ with $\boldsymbol{\lambda}$. The huge data scattering is caused by the dissimilar initial sphericities 0.45–0.85 of red **IBC/SCB** and 0.55–0.90 of white **IBC/SCB**. In addition, some scattering could result from the shorter transport path of the **IBC** released from the ephemeral streambed banks on the basin bed (see Faimon & Nehyba 2004).

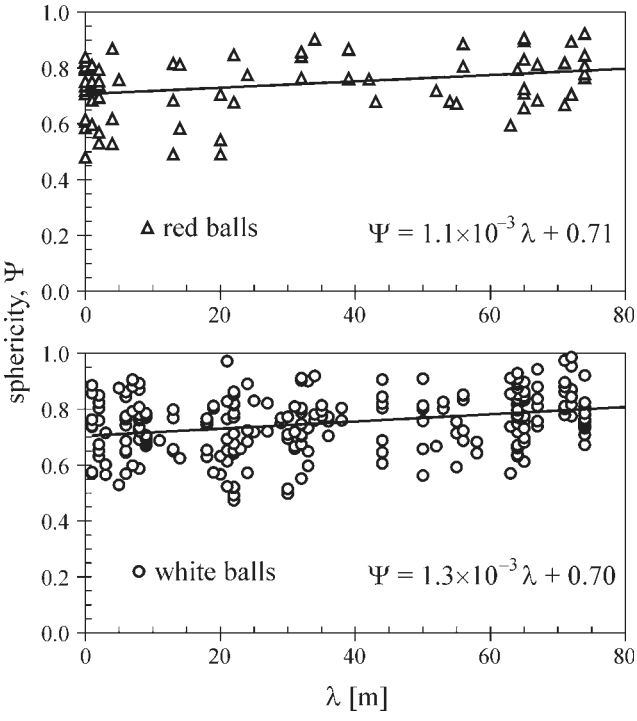

Fig. 5. Dependence of sphericity, $\mathbf{\Psi}$, on the distance from steep slope base, $\boldsymbol{\lambda}$.

Discussion

Data comparison

The found values of sphericity and effective diameter of **IBC/SCB** are consistent with those presented by Faimon & Nehyba (2004). This is not surprising because the localities were the same and conditions similar. Karcz (1969) reported analogous mud pebble sphericity; 0.6–0.7 near wadimouths and 0.55–1.0 near clayey wadi-banks. However, he referred to somewhat larger dimensions in comparison with the **IBC/SCB** in this study, from 4 to 10 cm in diameter. Based on findings of Faimon & Nehyba (2004), the **IBC/SCB** sizes are controlled by fissures in clays and by intensity of gully erosion. Ojakangas & Thomp-

son (1977) stated the dominance of spheroid mud balls at first appearance, but a majority of elliptical mud balls at second appearance, both in an urban environment. The size of these mud balls was lesser at the first appearance, from 1.0 to 2.3 cm, and significantly larger at the second appearance, the largest ball was about 25 cm long.

Discoid and bladelike mud balls, 4–25 cm long, were reported in the inter-tidal zone by Kale & Awasthi (1993). The preponderance of elongated mud balls ranging in size from 2 to 20 cm in diameter was also reported in the similar environment by Tanner (1996).

Mathematical model

A new model was derived to evaluate the **IBC/SCB** shaping at transport. The model is based on the principal assumption that the clay block shape is controlled by rotation of the IBC about a randomly changing axis (the axis orientation is presumed to be uniformly distributed on the interval [0, 2π]). The other assumptions are as follows: The sphericity ψ quantifies the instantaneous shape of clay ball. The condition $\psi = 1$ characterizes a "*steady state shape during transport*" (i.e. spherical shape). The deviation from the steady state shape is $1-\psi$. The high deviation (extremely irregular shape) will change more quickly than the slight deviation. Therefore, the increment of sphericity with number of rotations, $d\Psi/dn$, will be proportional to the deviation $1-\psi$,

$$\frac{d\Psi}{dn} = k\,(1-\Psi), \tag{4}$$

where **k** is a dimensionless constant.

The coefficient **k** itself includes the mechanical properties of the clay and basin bed. The possible effects of the **IBC/SCB** mass, runoff layer thickness, and runoff intensity were neglected (see discussion in Faimon & Nehyba 2004). Integrating the equation (4) in the initial conditions that $\Psi = \Psi_0$ if $n = 0$ (where Ψ_0 is the initial sphericity) gives

$$\Psi = 1 - (1-\Psi_0)\,e^{-k\,n}. \tag{5}$$

Other symbols have their standard meaning. The number of rotations, **n**, is a function of transport length and rotation perimeter. If the distance from the steep slope base, λ, is simply assumed to be a transport length, then

$$\lambda = p\,n, \tag{6}$$

where **p** is the rotation perimeter.

The question is how to evaluate the perimeter, **p**, unambiguously. This is rather difficult because the perimeter of non-spherical objects can vary during transport. For example, the perimeter of as simple and regular object as a cube can be very different, depending on whether the cube has rolled by the way of its "edges" or its "corners". Furthermore, the perimeter could decrease during transport if abrasion has operated. The dependence of d_{ef} on λ, is presented in Fig. 6. Actually, the negative slopes, –0.017 and –0.010 m m^{-1} for the red and white balls, respectively, indicate a slight decrease of the effective diameters with the distance from steep slope base. However, the R-square values, 0.071 and 0.045, document very weak correlation. Based on these facts, the decrease of d_{ef} was neglected and the effective diameter was assumed constant. This postulates that deformation dominates and abrasion is not significant.

The perimeter was expressed from the effective diameter as

$$p = \pi\, d_{ef}. \tag{7}$$

Inserting (7) into (6) gives

$$\lambda = \pi\, d_{ef}\, n. \tag{8}$$

Rewriting the equation (8) for **n** and inserting into (5) yields

$$\Psi = 1 - (1-\Psi_0)\,e^{-\frac{k\,\lambda}{\pi\, d_{ef}}}. \tag{9}$$

As can be seen, the equation (9) is only slightly modified in comparison with the equation (1). It authorizes the semi-empirical approach of Faimon & Nehyba (2004).

On the basis of the data processing, the constant **k** was determined. The logarithm of the equation (9) gives the expression

$$\ln(1-\Psi) = -\frac{k\,\lambda}{\pi\, d_{ef}} + \ln(1-\Psi_0), \tag{10}$$

representing the linear dependence of $\ln(1-\Psi)$ on λ/d_{ef} with the k/π slope. Plotting data in these coordinates (Fig. 7) and regressing by the equation (10) give the slopes 9.2×10^{-5} and 1.5×10^{-4}, from which **k** values, 2.9×10^{-4} and 4.8×10^{-4}, were calculated for the red and white clays, respectively. In Fig. 8, the theoretical functions (equation 9) are plotted for various initial sphericities. Despite the data scattering, a relatively good agreement of the calculated curves with the data points is visible.

Comparing the two models

Rewriting the equations (1) and (10) gives

$$\frac{d_{ef}}{\lambda}\log\left(\frac{\Psi-1}{\Psi_0-1}\right) = -\kappa \tag{11}$$

and

$$\frac{d_{ef}}{\lambda}\log\left(\frac{\Psi-1}{\Psi_0-1}\right) = -\frac{k\log e}{\pi}, \tag{12}$$

respectively. The symbol κ corresponds to the constant 8.9×10^{-5} from the previous model of Faimon & Nehyba (2004); **e** is the Euler number, the base of the natural logarithm. Comparing the right sides of the equations (11) and (12) yields

$$\kappa = \frac{k\log e}{\pi}. \tag{13}$$

Evaluating the former equation with the found **k** gives $\kappa \sim 4.0\times10^{-5}$ and 6.6×10^{-5} for the red and white clays, respectively. The two former values are somewhat lower

than the $\kappa \sim 8.9\times10^{-5}$ found by Faimon & Nehyba (2004) for the red clays. This difference could be a consequence of *changeable mechanical properties* of clays. For example, dry **IBC** needs a certain time to acquire its deformation ability. If heavy rains come after a long dry period, this ability can be reached after the initiation of transport. The calculation using the value of Faimon & Nehyba (2004), $\kappa = 8.9\times10^{-5}$, gives $\mathbf{k} = 6.4\times10^{-4}$. Therefore, the verified interval of the constant **k** for clay ball shaping is from 2.9×10^{-4} to 6.4×10^{-4}. The most probable value is $\mathbf{k} = (4.7 \pm 1.75)\times10^{-4}$.

Transport length estimation

Rewriting the equation (10) for $\boldsymbol{\lambda}$ gives the equation

$$\lambda = \frac{\pi\, d_{ef}}{k} \ln\left(\frac{1-\Psi_0}{1-\Psi}\right), \qquad (14)$$

which allows estimation of the minimal transport length so that the given shape was reached. Using the former value $\mathbf{k} = 4.7\times10^{-4}$, the calculation yields the transport length e.g. of 211, 105 and 53 m for the **IBC/SCB** of the effective diameters of 0.02, 0.01 and 0.005 m, respectively, so that the initial sphericity $\boldsymbol{\Psi}_0 = 0.75$ increases to $\boldsymbol{\Psi} = 0.95$.

Conclusions

The presented model is universal; it is valid for the description of spherical shape formation of various objects by transport (under the condition that orientation of rotation axis is uniformly distributed on the interval [0, 2π]). The model was derived for the transformation of small *irregular blocks of cohesive clay* (**IBC**) into *spherical clay balls* (**SCB**) during rolling under the effect of runoff. It was

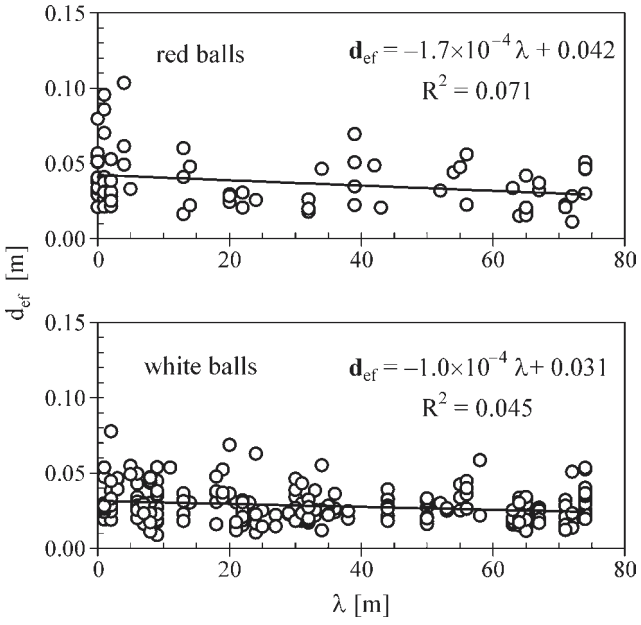

Fig. 6. Dependence of the effective diameter, $\mathbf{d}_{ef}$, on the distance from steep slope base, $\boldsymbol{\lambda}$.

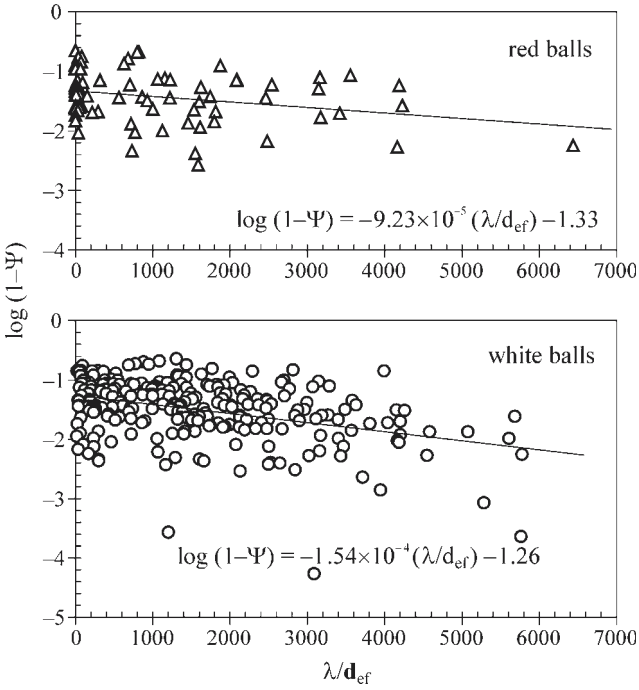

Fig. 7. Dependence of $\ln(1 - \boldsymbol{\Psi})$ on $\boldsymbol{\lambda}/\mathbf{d}_{ef}$.

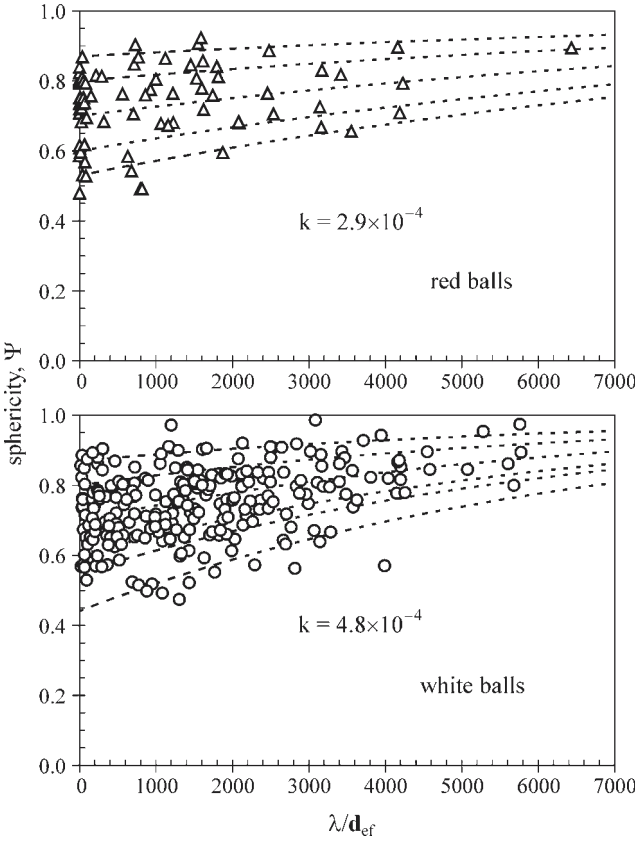

Fig. 8. Data fitting by the theoretical function.

based on the assumption that the change of shape with number of rotations depends on the deviation of observed shape from *steady state shape* (spherical). Clay deformation was found to control the shaping; abrasion seems to be less significant.

The model enables estimation of the length of transport, during which the **IBC** changed into the **SCB**. The parameter $\mathbf{k} = (4.7 \pm 1.75) \times 10^{-4}$ is valid for the sand/clayey environment. Although the shaping process was evaluated in artificial object (sandpit quarry), the model parameters are believed to be valid for analogous natural environment, such as clay rich cliffs and scarps in many settings worldwide.

Acknowledgments: The author wish to thank Dr. P. Čejchan and Prof. P. Bosák (Institute of Geology, Academy of Science of the Czech Republic), Prof. D. Vass (Geological Institute, Slovak Academy of Sciences), and two anonymous reviewers for their constructive comments. Dr. V. Vávra and P. Kadlec (Institute of Geological Sciences, Faculty of Sciences, Masaryk University) are thanked for performing of analyses.

References

Bell H.S. 1940: Armored mud balls — their origin, properties, and role in sedimentation. *J. Geol.* 48, 1–31.

Collinson J.D. & Thompson D.B. 1982: Sedimentary structures. *Alen & Unwin,* London, 1–194.

Bosák P., Glazek J., Gradzinski R. & Wojcik Z. 1976: Genesis and age of sediments of the Rudice type in fossil-karst depressions. *Čas. Mineral. Geol.* 24, 147–154.

Faimon J. & Nehyba S. 1998a: Recent formation of spherical mud balls at Rudice-Seč. *Geol. Res. in Morav. Siles. in 1997, ČGÚ, Masaryk. Univ.* 1, 2–3 (in Czech).

Faimon J. & Nehyba S. 1998b: The recent formation of spherical clay balls on sedimentary basin slopes. *Book of abstracts: 15th Conf. Clay Miner. Petrol., Sept. 3–10, 1998, Brno. Scripta Fac. Sci. Nat. Univ. Masaryk. Brun. (Geology)* 26, 1–76.

Faimon J. & Nehyba S. 2004: The formation of spherical clay balls on the slopes of sandpit quarry, the Rudice-Seč (Czech Republic). *Catena* 58, 23–40.

Haas W.H. 1927: Formation of clay balls. *J. Geol.* 35, 150–157.

Hindson R.A. & Andrade C. 1999: Sedimentation and hydrodynamic processes associated with the tsunami generated by the 1755 Lisbon earthquake. *Quart. Int.* 56, 27–38.

Kale S.V. & Awasthi A. 1993: Morphology and formation of armored mud balls on Revadanda Beach, Western India. *J. Sed. Petrology* 63, 809–813.

Karcz I. 1969: Mud pebbles in a flash floods environment. *J. Sed. Petrology* 39, 333–337.

Ojakangas R.W. & Thompson J.A. 1977: Modern armored mud balls in an urban environment. *J. Sed. Petrology* 47, 1630–1633.

Picard M.D. & High Jr. L.R. 1973: Sedimentary structures of ephemeral streams. In: Development in Sedimenology. Vol. 17. *Elsevier,* Amsterdam, 1–223.

Sholokhov V.V. & Tiunov K.V. 2002: The first finding of armoured mud balls in Turkmenistan. *Lithol. Miner. Resour.* 37, 92–93.

Sneed E.D. & Folk R.L. 1958: Pebbles in the lower Colorado River, Texas: a study in particle morphogenesis. *J. Geol.* 66, 114–150.

Tanner L.H. 1996: Armoured mud balls revisited. *Atl. Geol.* 32, 123–125.